Metal-insulator phase transition in the δ-(BEDT-TTF)4 [2,6-anthracene- bis(sulfonate)] $\times$4 H2 O studied by infrared spectroscopy

A. Frąckowiak, A. Łapiński, I. Olejniczak, R. Świetlik, D. Neubauer, W. Li, M. Dressel, M. Fourmigué, F. Camerel

Metal-insulator phase transition in the δ-(BEDT-TTF)$_4$[2,6-anthracene-bis(sulfonate)]·4H$_2$O studied by infrared spectroscopy

Arkadiusz Frąckowiak,[1,*] Andrzej Łapiński,[1] Iwona Olejniczak,[1] Roman Świetlik,[1] David Neubauer,[2] Weiwu Li,[2] Martin Dressel,[2] Marc Fourmigué,[3] and Franck Camerel[3]

[1]*Institute of Molecular Physics, Polish Academy of Sciences, ul. Mariana Smoluchowskiego 17, 60-179 Poznań, Poland*

[2]*1. Physikalisches Institut, Universität Stuttgart, Pfaffenwaldring 57, 70550 Stuttgart, Germany*

[3]*Univ Rennes, CNRS, Institut des Sciences Chimiques de Rennes (ISCR) UMR 6226, Campus de Beaulieu, 35042 Rennes, France*

[*]e-mail address: arkadiusz.frackowiak@ifmpan.poznan.pl

Temperature dependence of polarized infrared (IR) reflectance spectra of two-dimensional weakly dimerized organic conductor δ-(BEDT-TTF)$_4$[2,6-anthracene-bis(sulfonate)]·4H$_2$O with ¼-filled band has been measured to investigate the metal-insulator phase transition at T_{MI} = 85 K linked to charge ordering (CO). Vibrational bands related to C=C stretching vibrations of BEDT-TTF donor molecule give evidence of the CO and charge fluctuations both in the metallic and insulating phases above and below 85 K, respectively. Considerable modifications of the vibrational features due to electron-molecular vibration coupling are also observed. The phase transition is associated with the reorganization of hydrogen OH···O bonds in anion layers between the sulfonate moieties of the anion and the trapped water molecules, which is transmitted to conducting BEDT-TTF layers through weaker C-H···O bonds. The analysis of electronic bands confirms the presence of strong electronic correlations in the material. Two electronic absorptions are observed in the mid-IR region, attributed to transitions between Hubbard bands and transitions inside BEDT-TTF dimers. A low energy electronic absorption in the far-IR region is attributed to collective excitations of the short-range charge order. Below 85 K, the opening of a charge gap of ~24 meV is observed both parallel and perpendicular to the BEDT-TTF stacking direction. The spectroscopic data indicate that the CO phase transition is a consequence of both Coulomb interactions between charge carriers and donor-acceptor interactions.

I. INTRODUCTION

The organic donor bis(ethylenedithio)tetrathiafulvalene (BEDT-TTF or ET) with various acceptors forms many conducting quasi-two-dimensional charge transfer salts which exhibit a rich variety of electronic ground states, such as the Mott insulating state, charge ordering (CO), superconductivity, and quantum spin liquid … [1-3]. In this group of salts, the BEDT-TTF donor molecules in conducting layers are arranged in various structures described by Greek letters (e.g., *α, β, θ,* and *κ*). Because of the narrow bandwidth and low dimensionality, electronic correlations play an essential role; both onsite (*U*) and intersite (*V*) Coulomb repulsion energies should be considered. The parameter V is mainly responsible for forming the CO state in ¼-filled BEDT-TTF conductors (in terms of holes). The spatial distribution of charge-rich and charge-poor molecules inside layers depends on structural anisotropy and the intersite *V* interactions [4]. Subsequently, it was emphasized that donor-acceptor interactions, such as hydrogen and/or halogen bonding, can also play an essential role in the transition to the CO state. Therefore, the CO in BEDT-TTF salts should be considered as a consequence of both the Coulomb repulsion between charge carriers and the interactions between conducting BEDT-TTF and insulating acceptor layers [5-7].

The CO transition was observed in the ¼-filled two-dimensional BEDT-TTF salts with *α*, *β*, and *θ* type structures of conducting layers [3, 8, 9]. Recently, it was observed that the CO state also exists in a δ-phase BEDT-TTF salt, namely, δ-(BEDT-TTF)$_4$(ABS)·4H$_2$O [where ABS is 2,6-anthracene-bis(sulfonate)]. The material is metallic with room temperature conductivity of 100 Scm^{-1} and undergoes a metal-insulator phase transition at T_{MI} =85 K related with CO, and it is of first order [10]. As suggested by Raman spectroscopic studies, the uniform charge density distribution in the metallic phase (+0.5*e* per molecule) is modified <85 K so that there exist molecules with charges +0.7*e* and +0.3*e*. A characteristic structural feature of the salt is that the BEDT-TTF molecules in layers are organized in centrosymmetric dyads AA and BB, alternating along the *c* axis and the lateral *b* axis into a chessboard pattern (Fig. 1). Molecules within the dyads exhibit a ring-over-atom overlap mode and, between dyads, a twisted overlap mode; the twisted overlap mode is a specific feature of δ-phase BEDT-TTF salts [11]. The evaluation of the different HOMO···HOMO interaction energies has shown that the donor layers can be described as a series of parallel zigzag stacks of AB dimers [10]. Since the stacks are rather weakly dimerized, the salt can be considered as a ¼-filled system. The neighboring stacks interact through π- or σ-type interaction. Moreover, there exist important hydrogen bond interactions: weak C-H···O bonds between the donor and the sulfonate group of the anion and stronger bifurcated O-H···O bonds between the water molecules trapped within the anionic layer and the sulfonate groups. The metal-insulator transition at T_{MI} = 85 K is associated with the CO and modifications of the O-H···O bonds in acceptor layers which are transmitted to A and B donor molecules through the C-

H···O bonds [10]. Therefore, the metal-insulator CO transition in δ-(BEDT-TTF)$_4$(ABS)·4H$_2$O is exceptional for two reasons: this is not only an example of such a transition in δ-phase BEDT-TTF conductors, but it is also so clearly related with the contribution of donor-acceptor interactions.

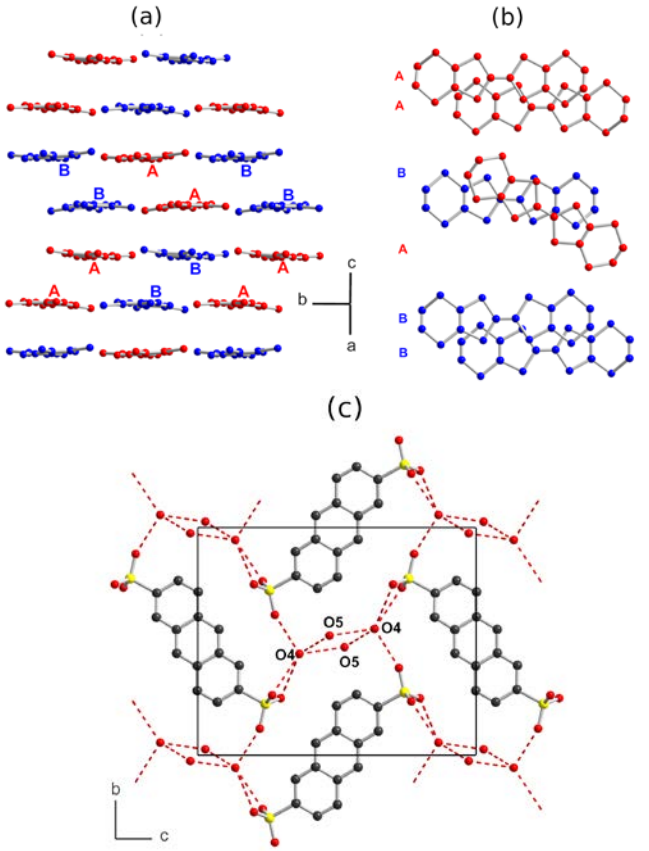

FIG. 1. Details of the structure of δ-(BEDT-TTF)$_4$(ABS)·4H$_2$O with (a) one BEDT-TTF layer with the two crystallographically independent molecules (noted A and B), (b) the overlap modes of neighboring donors, and (c) an anionic layer with hydrogen bonds (red dotted lines) between sulfonate groups of the ABS dianion and water molecules (O4, O5) [10].

The CO phenomena in low-dimensional organic conductors are commonly studied by infrared (IR) and Raman spectroscopies since some vibrational modes are very sensitive to charge residing on donor or acceptor molecules [3,8,9]. Additionally, in IR spectra, one can observe electronic bands which undergo significant changes due to CO metal-insulator transition, e.g., opening of a CO gap is seen in the far-IR region. In the case of charge-transfer salts based on tetrathiafulvalene (TTF) derivatives, the C=C stretching modes are especially sensitive for ionization degree. The flat BEDT-TTF in the D_{2h} point group symmetry has three C=C modes: $\nu_2(a_g)$= 1552 cm^{-1}, $\nu_3(a_g)$= 1494 cm^{-1}, and $\nu_{27}(b_{1u})$= 1505 cm^{-1} (for neutral molecule). When the ionization degree grows, the frequencies of these modes shift linearly toward lower frequencies so that, for BEDT-TTF$^+$ cations, they are observed at 1465, 1427, and 1398 cm^{-1}, respectively [8,9,12-14]. It has been shown that the IR active antisymmetric mode $\nu_{27}(b_{1u})$ is most useful for evaluation of charge. Nevertheless, in many cases, its observation is not an easy task because it is polarized along the long molecular axis which is usually nearly perpendicular to the BEDT-TTF layers, i.e., perpendicular to the best-developed crystal face [8, 9,14].

The aim of this paper is to shed more light on the specific nature of metal-insulator transition in the salt δ-BEDT-TTF)$_4$(ABS)·4H$_2$O, especially on the role played by donor-acceptor interactions.

II. EXPERIMENTAL

Single crystals of the salt δ-(BEDT-TTF)$_4$(ABS)·4H$_2$O were synthesized using electrochemical methods described previously [10]. The crystals were in the form of elongated plates of typical size 0.4 x 0.1 x 0.15 cm^3, with the best developed crystal face (100) parallel to the BEDT-TTF conducting layers. The optical axes of the studied samples were determined as those directions characterized by the largest anisotropy.

The polarized reflectance spectra were recorded in the 40-13000 cm^{-1} frequency range with the best resolution for each spectral range using Fourier-transform (FT)-IR spectrometers Bruker Equinox 55 and Bruker Vertex 80, together with an IR microscope Hyperion 1000 equipped with a set of polarizers. In the experiments, aluminum/silver/gold mirrors were used to obtain the absolute values of reflectance. At the lowest frequencies, the reflectance spectra were measured employing a Bruker IFS 113v FT spectrometer combined with a cold-finger cryostat and in situ gold evaporation as references [8]. The optical conductivity spectra were calculated from the reflectance spectra via the Kramers-Kronig transformation [15]. The low-frequency data, collected from the crystal face (100) parallel to the conducting layers, were extrapolated to zero frequency, assuming a Hagen-Rubens behavior for the metallic response. The low-frequency data in the polarization *E//a*, obtained from the crystal side face perpendicular to the BEDT-TTF layers, were extrapolated to zero frequency, assuming a constant value. The high-frequency data up to 10^6 cm^{-1} were extrapolated assuming ω^{-2} behavior, and the data beyond this frequency were extrapolated assuming a ω^{-4} behavior.

Raman spectra from the crystal side face with the electric field vector of the laser beam polarized parallel to the *a* axis (*E//a*) were measured in the 50-1700 cm^{-1} frequency range with a spectral resolution of 2 cm^{-1} in a backscattering geometry using a Raman spectrometer LABRAM HR800 equipped with a microscope. For excitation, we used a He-Ne laser ($\lambda_{exc.}$= 632.8 nm) with reduced power to <0.1 mW.

The IR and Raman spectra were measured in the temperature range T = 8-293 K in a continuous flow cold-finger cryostat manufactured by Oxford Instruments or a CryoVac He-flow cryostat. Good thermal contact was fulfilled with the help of vacuum grease. The cooling/heating rate was ≤1 K/min. The position and integral intensity of the vibrational bands were determined by a standard fitting technique using the PEAKFIT program.

III. RESULTS AND DISCUSSION

Figure 2 shows the room-temperature reflectance and optical conductivity of the δ-(BEDT-TTF)$_4$(ABS)·4H$_2$O salt in the frequency range 40-13000 cm^{-1}. For the electrical vector of the polarized light parallel (*E//c*) and perpendicular (*E//b*) to the stacking direction, the spectra were measured from the (100) crystal face, which is parallel to the conducting BEDT-TTF layers (in-plane polarization). The spectra for the perpendicular direction (*E//a*) were recorded from the side crystal face (out-of-plane polarization). The in-plane reflectance shows a metallike frequency dependence. At room temperature, a plasma edge is well pronounced only for the polarization parallel to the stacks (*E//c*) at ~5000 cm^{-1}. The reflectance for *E//c* in the mid-IR frequency range is slightly higher than that for *E//b*. For both in-plane spectra, one can see a relatively broad vibronic band at ~1200-1400 cm^{-1}, which is a consequence of the coupling of totally symmetric C=C modes of a_g symmetry with electrons [electron-molecular vibration (EMV) coupling]. The electronic band centered at ~8500 cm^{-1} can be assigned to charge-transfer between two charged BEDT-TTF molecules. On the other hand, for out-of-plane polarization (*E//a*), the reflectance is almost flat, but several vibrational features assigned to IR active BEDT-TTF and acceptor modes are well seen. The band at ~1220 cm^{-1} is related to stretching vibrations of SO_3^- groups in the anion layer; it is a band of the highest intensity for this polarization. The well-pronounced vibrational band at 1450 cm^{-1} is related to the charge-sensitive $\nu_{27}(b_{1u})$ mode, which is used to evaluate the charge density residing on the BEDT-TTF molecule [14]. The broad electronic band at ~11500 cm^{-1} for *E//a* is attributed to intramolecular BEDT-TTF excitation.

Temperature dependence of the in-plane reflectance and optical conductivity is displayed in Fig. 3. The reflectance and optical conductivity gradually grow on temperature lowering, which is a characteristic behavior for the metallike properties. This growth is much stronger for the spectra polarized perpendicular to the stacks (*E//b*) so

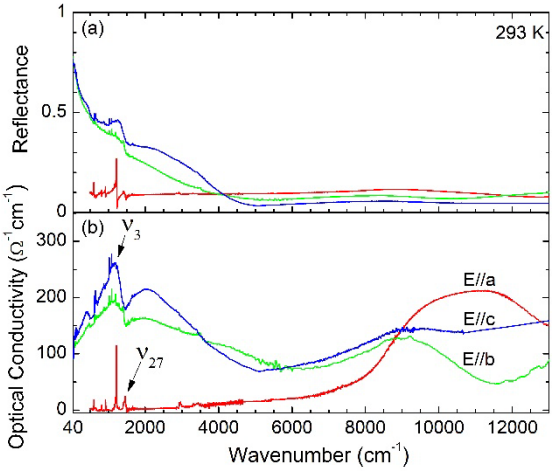

FIG. 2. (a) Polarized reflectance and (b) optical conductivity of the δ-(BEDT-TTF)$_4$(ABS)·4H$_2$O salt in the 40-13000 cm^{-1} frequency range at room temperature.

that, at low temperatures, a plasma edge clearly appears at ~3500 cm^{-1}. This behavior agrees with the increase of interstack side-by-side interactions observed by the crystallographic investigations [10]. The different edge positions for two perpendicular polarizations are ascribed to the anisotropic band structure. It is important that, in the far-IR region, no Drude response of the quasifree carriers is seen down to the phase transition temperature T_{MI} = 85 K.

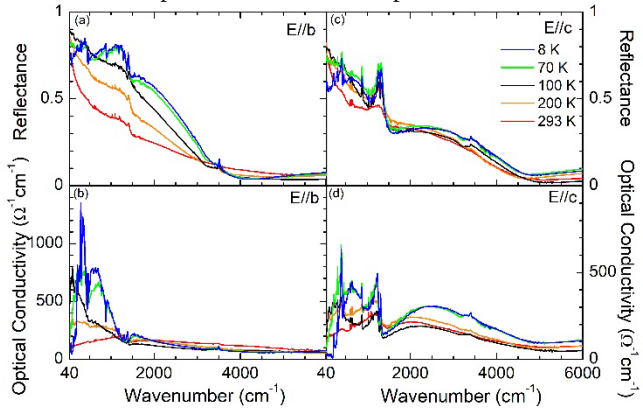

FIG. 3. Reflectance and optical conductivity spectra of δ-(BEDT-TTF)$_4$(ABS)·4H$_2$O as a function of temperature: in left panels (a) and (b), spectra are polarized perpendicular to the stacks, and in right panels (c) and (d), parallel to the stacks.

Below 85 K, the far-IR optical conductivity strongly drops, indicating clearly that a CO energy gap is opened, whose value grows on cooling (Fig. 4), and simultaneously, the spectral weight is transferred to higher frequencies. The far-IR optical conductivity jump was linearly extrapolated to evaluate the gap values: at T = 8 K in the stack

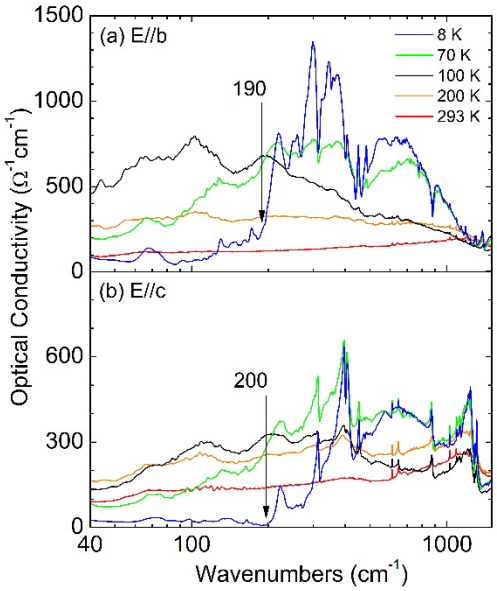

FIG. 4. Temperature dependence of the optical conductivity of δ-(BEDT-TTF)$_4$(ABS)·4H$_2$O <1500 cm^{-1}. In both polarizations, development of a charge-ordering (CO) energy gap is well seen. Arrows indicate the values of the energy gap (in cm^{-1}) at the temperature 8 K. Note the logarithmic frequency scale.

direction, 2Δ ~ 200 cm^{-1} (24.8 meV), and for perpendicular orientation, 2Δ ~ 190 cm^{-1} (23.6 meV). The optical gap is nearly the same in both directions; however, it is disturbed by several vibrational features. Simultaneously, <85 K, the EMV spectral features in the region 1200-1400 cm^{-1} increase their intensities for both polarizations (Fig. 3). All bands observed in the optical conductivity spectra of δ-(BEDT-TTF)$_4$(ABS)·4H$_2$O at room temperature were assigned and collected with bands observed in the Raman spectra at 293 K and with calculated frequencies of ABS (Tables S1 and S2 in the Supplemental Material [16]).

A. CO study by vibrational features

The temperature dependence of the charge-sensitive mode $\nu_{27}(b_{1u})$ is shown in Fig. 5. Above T_{MI} = 85 K, we observe a relatively broad band centered at ~1450 cm^{-1}, and <85 K, an additional band centered at ~1477 cm^{-1} develops [Fig. 5(a)]. On closer inspection of the 1450 cm^{-1} feature, we see that, at ambient temperature, it consists of several components, i.e., lines at 1445 cm^{-1} (***1***) and 1454 cm^{-1} (***2***), and on the right-side slope, weaker lines at 1464 cm^{-1} (***3***) and 1475 cm^{-1} (***4***). In Fig. S1 in the Supplemental Material [16], the band decomposition is presented. Due to the phase transition, the spectrum undergoes significant modifications: bands ***1*** and ***4*** abruptly increase the intensities, while the band ***2*** abruptly decreases the intensity. Moreover, band ***1*** shifts towards lower frequency, and bands ***2***, ***3***, and ***4*** shift toward higher frequency [Fig. 5(b)]. Consequently, at T = 8 K, we see four lines at 1443, 1461, 1467, and 1477 cm^{-1}. At room temperature, the band at 1416 cm^{-1} is attributed to the IR active C-H$_2$ bending $\nu_{28}(b_{1u})$ and $\nu_{45}(b_{2u})$ modes and is almost insensitive to temperature variation.

One can evaluate the charge (ρ) on BEDT-TTF using the following well-known formula [14]:

$$\nu_{27}(\rho) = 1398 \text{ cm}^{-1} + 140\,(1-\rho) \text{ cm}^{-1} \quad (1)$$

At ambient temperature, the various components of $\nu_{27}(b_{1u})$ correspond to fractional charges: +0.64e (***1***), +0.58e (***2***), +0.53e (***3***), and +0.46e (***4***), while at 8 K they correspond to the charges +0.68e, +0.55e, +0.50e, and +0.43e, respectively. It is well seen that, already at ambient temperature, the charge ρ is not distributed uniformly among BEDT-TTF molecules, i.e., there exist significant pre-transitional fluctuations of the charge distribution which are observed up to room temperature at least. Due to a charge redistribution <85 K, the concentration of molecules with charges +0.68e and +0.43e abruptly grows (CO insulating phase); however, there still exist also molecules with charges +0.55e and +0.50e (metallic phase). The charge-rich BEDT-TTF molecule, marked as mol. A at room temperature, changes into a charge-poor molecule <85 K. At 8 K, the BEDT-TTF molecule, marked as mol. B becomes a charge-rich molecule [10].

In the metallic phase, >85 K, the observed average charge on BEDT-TTF is > +0.5e, which is the value resulting from the stoichiometry. Indication of charge disproportionation in the metallic phase was also observed in other BEDT-TTF charge-transfer salts [17,18]. It was regarded as a precursor of the charge ordered ground state. However, the origin of the presence of charges different to +0.5e in the metallic phase of organic conductors is still not clear. The discrepancy

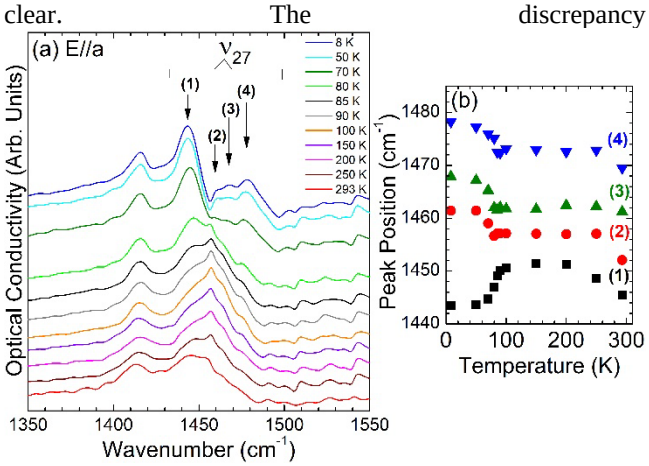

FIG. 5. (a) Optical conductivity spectra of δ-(BEDT-TTF)$_4$(ABS)·4H$_2$O in the frequency range of the ν_{27} mode for selected temperatures. (b) Positions of the ν_{27} components as a function of temperature.

in δ-(BEDT-TTF)$_4$(ABS)·4H$_2$O can be due to strong donor-acceptor interactions (hydrogen bonding and/or electrostatic interactions with SO_3^- groups) that may yield some frequency shifts of vibrational modes. Moreover, the existence of two separated bands ***2*** and ***3*** gives evidence that charge is not distributed uniformly among molecules A and B, even at ambient temperature. We should emphasize that the nonuniform charge distribution was already inferred from the crystallographic data: +0.52*e* on A and +0.48*e* on B at T = 300 K [10]. An analogous situation exists <85 K: if we assign the lines at 1461 cm^{-1} (***2***) and 1467 cm^{-1} (***3***) to remnants of the metallic phase, the average charge is also different from +0.5*e* and distributed nonuniformly. For these reasons, it is more convenient to use the charge difference between molecules 2δ. Above 85 K, the charge distribution fluctuates between 2δ = +0.05*e* and 2δ = +0.19*e*, but at 8 K it fluctuates between 2δ = +0.08*e* and 2δ = +0.25*e*. For the metallic phase, the difference between A and B molecules (2δ = +0.05*e*) and for the insulating CO phase (2δ = +0.25*e*) is nearly in agreement with the crystallographic data (2δ = +0.04*e* at 300 K and 2δ = +0.20*e* at 15 K [10]). Apart from Coulomb interactions between charge carriers, strong donor-acceptor interactions contribute to the CO. The nonuniform charge distribution in BEDT-TTF layers, observed already at ambient temperature, supports this suggestion.

To verify the above conclusions, additional measurements of Raman spectra with the laser beam focused on the same crystal side face were performed. The charge sensitive C=C stretching mode $\nu_2(a_g)$ that is also used to study the charge distribution was analyzed [8,9,14] (Fig. S2 in the Supplemental Material [16]). Above 85 K, we see the band $\nu_2(a_g)$ at 1496 cm^{-1} (charge +0.59*e*) and, <85 K, two $\nu_2(a_g)$ bands at 1484 and 1514 cm^{-1} (charges +0.69*e* and +0.44*e*). These bands are rather weak and broad; therefore, they exhibit no visible structure. Nevertheless, the Raman data support our conclusions resulting from IR studies. We recall that our previous studies of Raman spectra carried out for the laser beam focused on the crystal face (100), parallel to the conducting layers, gave in the CO phase <85 K the charges +0.7*e* and +0.3*e* [10].

The CO has also a considerable influence on other IR vibrational features. Temperature dependence of in-plane optical conductivity in the region of C=C stretching modes is displayed in Figs. 6(a) and 6(b). For polarization parallel to the stacks (*E//c*), we observe a broad and robust spectral feature in the 1100-1300 cm^{-1} frequency range [Fig. 6(a)], which is attributed to the totally symmetric C=C stretching mode $\nu_3(a_g)$ activated by coupling with electrons inside weakly dimerized BEDT-TTF stacks (face-to-face EMV coupling). Interestingly, the $\nu_3(a_g)$ mode is also well seen in the perpendicular polarization (*E//b*) at 1398 cm^{-1} (293 K), which is activated by the EMV coupling with the side-by-side charge-transfer transition between neighboring stacks [Fig. 6(b)]. On cooling, this band shifts toward lower frequencies down to 1380 cm^{-1} at 8 K, and its intensity strongly increases below the T_{MI} = 85 K, providing thus evidence of an increase of the interstack interactions due to the phase transition [Fig. 6(c)], in agreement with the calculations of HOMO···HOMO interaction energies [10]. In both polarizations, we see two features at 1290 and 1308 cm^{-1} [Figs. 6(a) and 6(b)] assigned to the $\nu_5(a_g)$ mode, associated with C-H bending vibrations of the ethylene groups. The mode is observed as two dips in the *E//c* polarization and as two peaks in the *E//b* polarization. The doublet structure suggests the existence of nonequivalent molecules, e.g., with various charges and/or donor-acceptor interactions. At 85 K, both the integral intensity [Fig. 6(d)] and position [Fig. 6(e)] of the $\nu_5(a_g)$ mode undergo abrupt changes only for polarization perpendicular to the stacks (*E//b*). On the other hand, for parallel polarization, both parameters change continuously with lowering temperature. Temperature dependence of the $\nu_5(a_g)$ mode is analogous to the $\nu_3(a_g)$ mode for the same polarization, supporting thus the previous conclusion that the modifications of interstack interactions are an important consequence of the phase transition.

The BEDT-TTF mode at ~890 cm^{-1} was originally assigned as $\nu_{60}(b_{3g})$ for a flat molecule in the D_{2h} point group symmetry [12,13] and then discussed as the totally symmetric $\nu_{10}(a)$ mode for a distorted molecule in the D_2 point group symmetry [19,20]. By now, it is established that the 890 cm^{-1} mode is very sensitive to both chemical and physical tuning in a wide variety of BEDT-TTF salts [21].

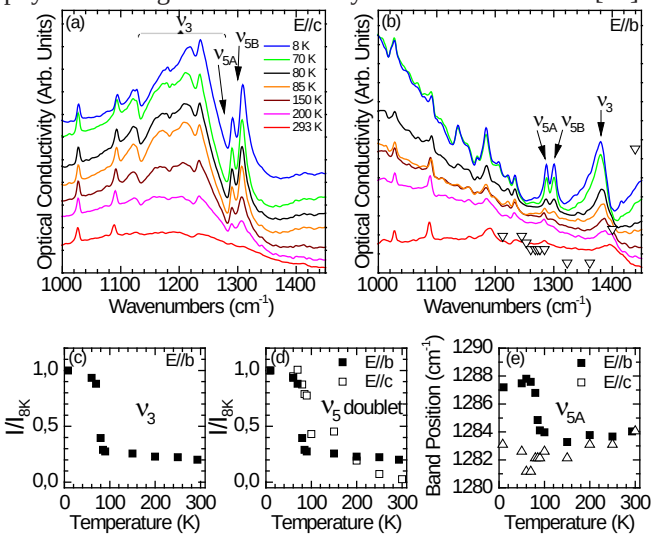

FIG. 6. (a) *c*-polarized and (b) *b*-polarized optical conductivity spectra of δ-(BEDT-TTF)$_4$(ABS)·4H$_2$O in the frequency range of C=C stretching vibrations at selected temperatures; (c) temperature dependence of the normalized integral intensity of the ν_3 band measured for polarization perpendicular to the BEDT-TTF stacks and (d) the doublet of ν_5 bands for both polarizations; (e) temperature dependence of the position of the ν_{5A} band for both polarizations.

Assuming a reduced local symmetry of BEDT-TTF (D_2 point group), the ring breathing mode ν_{10}(a) is predicted to display strong vibronic coupling, and it was shown that such interaction really exists [19,20]. In our IR spectra, this mode is observed as a dip with two components at 880 and 892 cm^{-1} which develops at lower temperatures for polarization perpendicular to the stacks [polarization *E//b*, Fig. 7(a)]. Analogously, for the stack polarization (*E//c*), one can see a band at 873 cm^{-1} accompanied by a weaker feature at 892 cm^{-1} [Fig. 7(b)]. For both polarizations, the intensity of this mode drastically increases below the phase transition temperature [Fig. 6(c)]. If we consider that vibrational features related to the $\nu_{60}(b_{3g})$ mode [or rather ν_{10}(a) mode for D_2 symmetry] are a consequence of EMV coupling, the temperature dependence of their integral intensities gives evidence that the phase transition modifies both intrastack and interstack interactions.

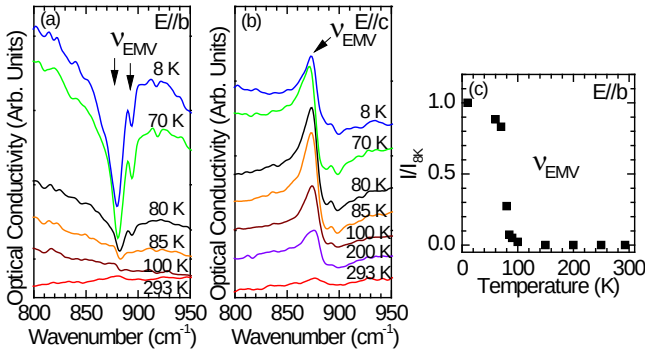

FIG. 7. Temperature dependence of (a) *b*-polarized and (b) *c*-polarized optical conductivity spectra of δ-(BEDT-TTF)$_4$(ABS)·4H$_2$O in the frequency range of the ν_{60} mode. (c) Temperature dependence of the normalized integral intensity of the ν_{60} mode (marked as ν_{EMV}).

It has been shown that, from the structural point of view, in similar materials β-(BEDT-TTF)$_2$X (where X = IBr_2, AuI_2, I_3), hydrogen interaction within the anion layer as well as between cation and anion layers influence effectively on the electronic properties [22]. Similar conclusions appear also from optical measurements performed to the ½-filled κ-BEDT-TTF salts [23]. First-principles density functional theory calculations that were performed to two-dimensional ¼-filled α-BEDT-TTF salt enhance the outcome of experimental studies about the crucial role that an anion plays on physical properties in charge-transfer salts [5].

Our previous paper [10] showed that the metal-insulator transition is accompanied by considerable modifications of the hydrogen bond network, formed inside insulating anion layers between the sulfonate groups SO_3^- of anions and the trapped water molecules. These modifications are transmitted through weaker hydrogen bonds to the conducting BEDT-TTF layers. Therefore, it is to be expected that these modifications should have an influence on C-H stretching vibrations of the ethylene groups of BEDT-TTF. Similarly, the SO_3^- vibrations of acceptors and O-H vibrations of water molecules inside the anion layers should be also modified due to the phase transition. Figure 8(a) presents the out-of-plane optical conductivity spectra in the region of SO_3^- modes for selected temperatures. The temperature dependence of the SO_3^- feature shows that it consists of three components. With lowering temperature, two of three components shift abruptly toward higher frequencies <85 K [Fig. 8(c)]. It is related to shortening of every two S=O bonds from the SO_3^- group below the metal-insulator phase transition that excellently agrees with the x-ray bond-length study [10].

On the other hand, Fig. 8(b) shows the in-plane optical conductivity for polarization perpendicular to the stacks (E//b) in the region of O-H stretching. We observe the band at 3483 cm^{-1} at 293 K marked as ν_β which shifts gradually towards higher frequencies upon cooling, reaching 3499 cm^{-1} at 8 K [Fig. 8(d)]. Moreover, for E//b, the ν_α band develops <~200 K (3401 cm^{-1} at 150 K). Due to the phase transition, its frequency jumps abruptly up to 3409 cm^{-1} at 70 K [Fig. 8(d)]. In Fig. 8(b), we see also that the ν_α and ν_β lines are superimposed on a broad band (between 3150 and 3650 cm^{-1}), which develops <~200 K and exists down to ~50 K. This spectral feature should be attributed to vibrations of disordered O-H groups involved in O-H···O hydrogen bonds. As shown by the crystallographic data [10], the phase transition is related with considerable reorganization of the hydrogen bond network in anion layers. This network can exhibit a disorder in the temperature range where the pre-transitional effects are observed both above and below T_{MI}. The temperature dependence of the bands ν_α and ν_β, as well as of the broad feature 3150-3650 cm^{-1}, provides clear evidence of reorganization of the hydrogen bond network. Moreover, this reorganization does not happen abruptly, but it is extended over a broad temperature range and is associated with strong disorder. Similar effects are observed for polarization parallel to the stacks (*E//c*) (Figure S3 in the Supplemental Material [16]). On the other hand, the C-H stretching bands of the ethylene groups, though clearly detected in IR spectra, are too weak to study their temperature dependence.

B. Charge order fluctuations study

The relatively broad ν_{27} features observed in the spectra of δ-(BEDT-TTF)$_4$(ABS)·4H$_2$O in the 8-293 K temperature range suggest the presence of charge fluctuations (in the time domain) in high- and low-temperature regimes. The single structured ν_{27} band splits into two features at ~80 K that are also structured. It suggests that charge distribution in δ-(BEDT-TTF)$_4$(ABS)·4H$_2$O is quite complex, and probably two regimes are present. Hence, the charge distribution in the donor layers can be understood by assuming that the charge stochastically jumps between two crystallographically independent molecules, i.e., mol. A and mol. B, respectively.

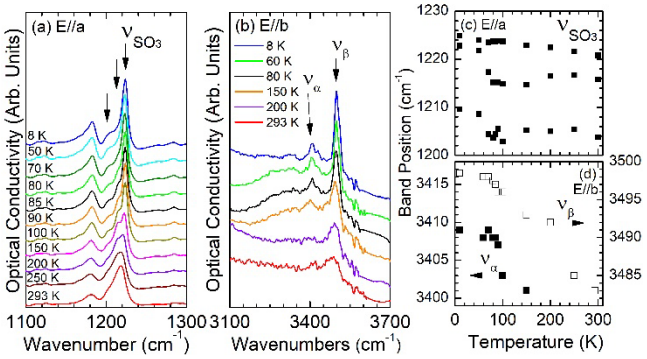

FIG. 8. Temperature dependence of (a) *c*-polarized and (b) *b*-polarized optical conductivity spectra of δ-(BEDT-TTF)$_4$(ABS)·4H$_2$O in the frequency range of stretching vibrations of S=O and hydrogen bonds, respectively. (c) Temperature dependence of ν_{SO3} components and (d) ν_α and ν_β bands in the optical conductivity spectra of δ-(BEDT-TTF)$_4$(ABS)·4H$_2$O in polarization *E//b*.

We adopted the Kubo model to account for band shape and frequency of the ν_{27} mode in the two different regimes [9,24,25]. The Kubo model function is given by the real part of the following complex function:

$$\mathcal{L}(\omega) = \frac{\mathcal{F}[(\gamma+2\nu_{ex})-i(\omega-\omega_w)]}{\mathcal{R}^2-(\omega-\omega_A)(\omega-\omega_B)-2i\Gamma(\omega-\omega_{av})}, \quad (2)$$

where $\boldsymbol{\mathcal{F}} = f_A + f_B$ (f_A, f_B are the oscillator strengths of the bands of the ω_A and ω_B frequencies and half-width γ); the velocity of the charge fluctuation is ν_{ex}, and the sum of the intrinsic width γ and the exchange rate ν_{ex} is given by $\Gamma=\gamma+\nu_{ex}$; $\boldsymbol{\mathcal{R}}^2 = 2\gamma\nu_{ex} + \gamma^2$; ω_{av} is the average frequency and is equal to $\omega_{av} = \frac{\omega_A+\omega_B}{2}$, and the weighted frequency is equal to $\omega_w = \frac{f_B\omega_A+f_A\omega_B}{f_A+f_B}$. If the exchange component $\nu_{ex}\ll|\omega_A-\omega_B|/2$, then $\boldsymbol{\mathcal{L}}(\omega)$ yields two separated bands centered at ω_A and ω_B, but if $\nu_{ex} \gg|\omega_A-\omega_B|/2$, then it yields one single band centered at ω_{av}. The spectral weight of one broad band shifts toward the higher oscillator strength mode when $\nu_{ex} \approx |\omega_A-\omega_B|/2$. Fitting of the registered spectra with the $\boldsymbol{\mathcal{L}}(\omega)$ function puts forward the ω_A and ω_B frequencies that are related to partial charge localized on molecules A and B, the oscillator strengths ratio, and the charge fluctuations velocity. The fitting in the IR range is constrained [20].

Figure 9 presents the fits of the IR spectra of δ-(BEDT-TTF)$_4$(ABS)·4H$_2$O at 8 K and 200 K, respectively, below and above the metal-insulator phase transition. In the high-temperature phase at 200 K [Fig. 9(a)], the single broad ν_{27} band is fitted by the superposition of two Lorentz oscillators, due to the mode relevant to a static charge disproportionation, respectively, charge-rich (red line) and charge-poor (blue line) features, one band shape function $\boldsymbol{\mathcal{L}}(\omega)$ (green line) that is related to surviving fluctuation regime and two Lorentzian bands associated with charge-unrelated $\nu_{28,45}$ modes. Two Lorentzians that correspond to static CO are centered at $\omega_{mol.A}$=1443 cm^{-1} and $\omega_{mol.B}$=1476 cm^{-1} with $\rho_{mol.A}$=+0.68*e* and $\rho_{mol.B}$=+0.44*e*, respectively. The band shape function $\boldsymbol{\mathcal{L}}(\omega)$ is observed as a broad two-component feature, and the parameters of the fluctuating regime are the following: $\Delta\omega$=29 cm^{-1}, $2\delta_{Kubo}$=+0.21*e*, $\nu_{ex}\approx$13 cm^{-1}. It shows that fitting of the broad feature in the 1300-1500 cm^{-1} range by Lorentz functions is possible even in the fluctuation regime because the value of exchange velocity is much smaller than the frequency difference between charge-rich and charge-poor states. All fitted parameters are presented in Tables S3 and S4 in the Supplemental Material [16].

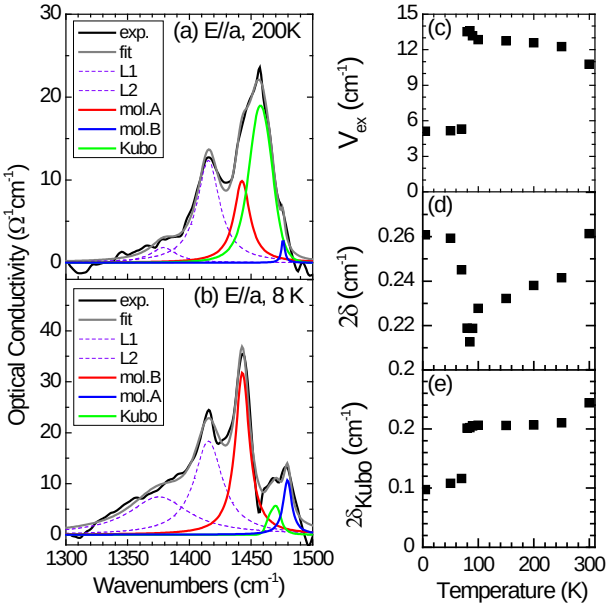

FIG. 9. Fit of the charge-sensitive ν_{27} mode in the optical conductivity spectra of δ-(BEDT-TTF)$_4$(ABS)·4H$_2$O at (a) 200 K and (b) 8 K (b) in two CO regimes using Kubo model. (c) Velocity of charge fluctuation, (d) static, and (e) dynamic charge disproportion as a function of temperature estimated from infrared (IR) spectra using Kubo model.

In the low-temperature phase at 8 K, the fitted spectrum of δ-(BEDT-TTF)$_4$(ABS)·4H$_2$O consists of the same components; however, two Lorentzians related to static CO are centered at $\omega_{mol.B}$=1443 cm^{-1} and at $\omega_{mol.A}$=1480 cm^{-1}, and function $\boldsymbol{\mathcal{L}}(\omega)$ is observed as a two-band feature [Fig. 9(b)]. The fit parameters of the fluctuation regime are $\Delta\omega$=14 cm^{-1}, $2\delta_{Kubo}$=+0.1*e*, and $\nu_{ex}\approx$5 cm^{-1}. With lowering temperature, the exchange component in δ-(BEDT-TTF)$_4$(ABS)·4H$_2$O changes dramatically around the phase transition [Fig. 9(c)]. Between 100 and 8 K, the ν_{ex} drops from 13 to 5 cm^{-1}. It suggests that, in δ-(BEDT-TTF)$_4$(ABS)·4H$_2$O, fluctuations slow down significantly upon cooling. The fluctuation velocity does not go to zero. This indicates that the metal-insulator phase transition is not fully completed. Moreover, with lowering the temperature,

the value of static charge disproportionation behaves differently above and below phase transition temperature [Fig. 9(d)]. Increase of the 2δ parameter at the metal-insulator phase transition implies that the value of charge disproportionation grows proportionally to electronic correlations. Significant change of charge disproportionation is also observed in the fluctuation regime. Below 100 K, $2\delta_{Kubo}$ drops from +0.2*e* to +0.1*e* at 8 K [Fig. 9(e)].

Temperature dependence of exchange velocity in δ-(BEDT-TTF)$_4$(ABS)·4H$_2$O calculated with the Kubo model is like that observed in β''-(BEDT-TTF)$_2$SF$_5$CH$_2$CF$_2$SO$_3$, where the coexistence of fluctuating and static CO is also observed [25]. The ν_{ex} in δ-(BEDT-TTF)$_4$(ABS)·4H$_2$O significantly decreases with lowering temperature; however, the values are roughly two times smaller in comparison with the β''-salt. Suppression of charge fluctuation with lowering temperature is characteristic of a first order metal-insulator phase transition. At the same time, the "frozen" CO related to static charge disproportionation also emerges. It was suggested that such behavior yields when the sample is placed in the mixed phase on the phase diagram of ¼-filled BEDT-TTF salts [25,26]. The presence of the mixed phase that is on the border between insulating and metallic phases is related to competition of two almost orthogonal types of charge-order developing states – the fluctuating CO between the stacks and the frozen CO along the stacks [25]. Moreover, it was highlighted that the coexistence is not related to presence of macroscopic domains at the borderline between the phases and cannot be predicted with mean field theories. In δ-(BEDT-TTF)$_4$(ABS)·4H$_2$O, we observe relatively high oblique interactions that increase together with development of static CO. With increase of this type of interaction, the order in the anion layer develops. In effect, transfer integrals in donor layers increase more effectively than Coulomb interactions; it happens when the lattice is contracted and the bandwidth increases at the expense of suppression of the CO transition [17,27]. On the other hand, anion ordering may induce a reduction of dynamical fluctuation of inhomogeneously distributed short-range CO stripes that could be potentially present in δ-(BEDT-TTF)$_4$(ABS)·4H$_2$O as it was suggested in the case of α-(BEDT-TTF)$_2$I$_3$ [17].

C. Electronic spectra

The electron correlations have a significant influence on the electronic spectra of low-dimensional ¼-filled BEDT-TTF salts; particularly, in electronic transitions between Hubbard bands, opening of the charge-order gap and charge-order fluctuations are observed [8,25,26,28-33]. As seen in Fig. 3, the CO strongly modifies the in-plane electronic spectra of the salt δ-(BEDT-TTF)$_4$(ABS)·4H$_2$O. The most important effect, observed both in the direction parallel and perpendicular to the stacks, is that below T_{MI} = 85 K, the energy gap develops with a value that grows on further cooling (Fig. 4). Simultaneously, the spectral weight shifts to the mid-IR range. We relate the energy gap of ~24 meV to CO due to electronic correlations, most probably with a substantial contribution of donor-acceptor interaction. The band structure calculations also revealed the gap opening: it equals 28 meV at 80 K and increases up to 50 meV at 15 K [10]. This is a quite satisfactory agreement with the gap evaluated from spectroscopic data since extrapolation to zero conductivity is rather arbitrary (Fig. 4). The experimental gap in our material is ~3 times smaller than the charge-order gap in the salt α-(BEDT-TTF)$_2$I$_2$ (74 meV [34]) and the salt β"-(BEDT-TTF)$_2$Hg(SCN)$_2$Cl (60 meV [35]).

Above T_{MI}= 85 K, the salt exhibits a metallic temperature dependence of the resistivity. However, no Drude-like peak is observed in the in-plane optical conductivity in the far-IR range, i.e., there exist no coherent Landau quasiparticles expected for ordinary metals (Fig. 3). Therefore, the studied compound should be classified as a "bad metal", the behavior often observed in conducting low-dimensional charge-transfer salts with strong electron correlations [8,28,30,36].

The strongly correlated character of the salt is also manifested in the spectral weight, which exhibits different behavior compared with ordinary metals. The frequency-dependent spectral weight is given by the following formula:

$$I_\sigma(\omega_c) = \int_0^{\omega_c} \sigma_1(\omega) d\omega = \frac{\pi e^2}{2m^*_{sum}} n(\omega_c), \qquad (3)$$

where ω_c is the cutoff frequency, m^*_{sum} is the effective mass, and $n(\omega_c)$ is the density of carriers contributing to the optical conductivity up to ω_c. Our attention was focused on the spectral range up to 6000 cm^{-1}. The total spectral weight as a function of cutoff frequency for different temperatures is displayed in Fig. 10 (left panel). In Fig. 10, in both polarizations, we see small steps at ~500 and 1200 cm^{-1} related to BEDT-TTF vibrations interacting strongly with electrons (EMV coupling). The redistribution of the spectral weight over a broad frequency range is typical for organic conductors showing bad metal behavior. As seen in Fig. 10(c), from room temperature down to 8 K, the center of the spectral weight is strongly shifted toward lower frequencies only for the polarization perpendicular to the stacks (*E//b*), i.e., the direction of strong modifications of intermolecular interactions, in agreement with the x-ray structural data [10] and above analysis of vibrational features (point 3.1).

The in-plane optical spectra of δ-(BEDT-TTF)$_4$(ABS)·4H$_2$O at room temperature are dominated by a broad electronic absorption centered at ~2000 cm^{-1} (Fig. 2). On cooling, this absorption is modified, and on closer examination, one can easily see that it contains several components (Fig. 3). To separate the various contributions to the electronic absorption and to study their temperature behavior, we have performed deconvolution of the bands by using Lorentz functions for the complex conductivity:

$$\hat{\sigma}(\omega) = \frac{Ne^2}{m_0} \frac{\omega}{i(\omega_0^2 - \omega^2) + \gamma\omega} \qquad (4)$$

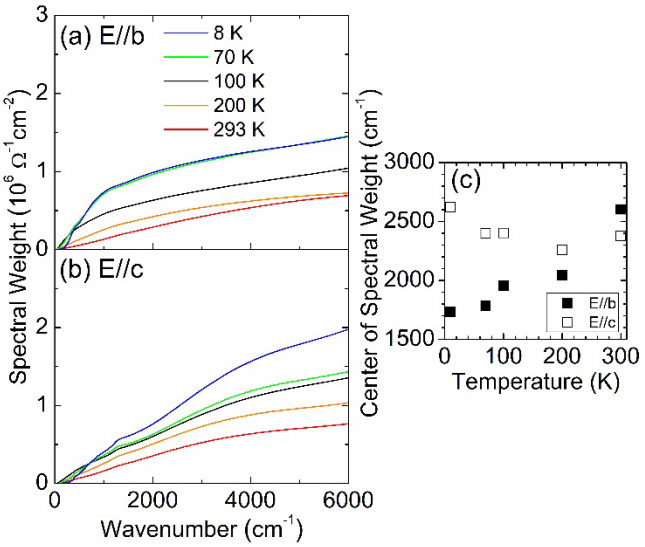

FIG. 10. Temperature dependence of the spectral weight of δ-(BEDT-TTF)$_4$(ABS)·4H$_2$O for polarization (a) perpendicular and (b) parallel to the stack for selected temperatures. (c) Temperature dependence of the center of the spectra weight for both polarizations in the 40-6000 cm^{-1} frequency range.

where N is the number of charge carriers, m_0 is the band mass, ω_0 is the oscillator frequency, γ is the linewidth. As an example, in Fig. 11, we display the band deconvolution at T = 8 K. For polarization parallel to the stacks (*E//c*), the electronic absorption has been decomposed into five bands [P_1, P_2, P_{EMV}, P_3, and P_4 – see Fig. 11(a)], whereas for perpendicular polarization (E//b), it has been decomposed into four features [P_1, P_2, P_3 and P_4 – Fig.11(b)]. We assign these bands to the following processes: P_1 is a short-range CO fluctuation, P_2 is an electron transition between the electronic states at the Fermi level and the Hubbard bands, P_{EMV} is a vibrational feature due to coupling of the ν_3 mode with electrons [it is only important for *E//c* – see Fig. 11(a)], P_3 is the electron transition between the Hubbard bands, and P_4 is the intradimer (*E//c*) or interstack (*E//b*) excitation. The frequencies of the mid-IR features fitted with Lorentz functions at 8 and 293 K are listed in Table 1. Temperature dependence of the frequencies of bands, their half-width, and amplitude in polarizations *b* and *c* are, respectively, shown in Figs. S4 and S5 in the Supplemental Material [16]. The phase transition has a significant influence on some bands. It should also be noticed that the lower-frequency electronic absorptions are strongly distorted by intense vibrational features.

TABLE 1. Frequencies (cm^{-1}) of the centers of electronic features determined by the Lorentz function fits of the δ-(BEDT-TTF)$_4$(ABS)·4H$_2$O optical conductivity spectra.

Band	293 K		10 K	
	E//c	E//b	E//c	E//b
P_1	330	600	390	320
P_2	860	1140	680	670
P_{EMV}	1160	-	1190	-
P_3	2050	2070	2330	1680
P_4	2580	2910	3420	3430

The electronic properties of the ¼-filled BEDT-TTF salts have been successfully described in terms of the extended Hubbard model - as emphasized above, the intersite Coulomb repulsion V gives rise to a CO ground state [8,25,26,29,34,35]. The intradimer electronic transition P_4 is centered at ~2580 cm^{-1} (at 293 K) for polarization parallel to the stacks (*E//c*) and is the charge transfer between molecules A and B. The band P_{EMV} is a consequence of the coupling of P_4 with the C=C stretching mode ν_3. Interestingly, for perpendicular polarization (*E//b*), one can also see the electronic transition P_4 at ~2910 cm^{-1} (at 293 K), which also couples with the mode ν_3 yielding a much weaker vibrational feature at 1398 cm^{-1} [Fig. 6(b)]. The band P_4 at 2910 cm^{-1} should be related to interstack transitions.

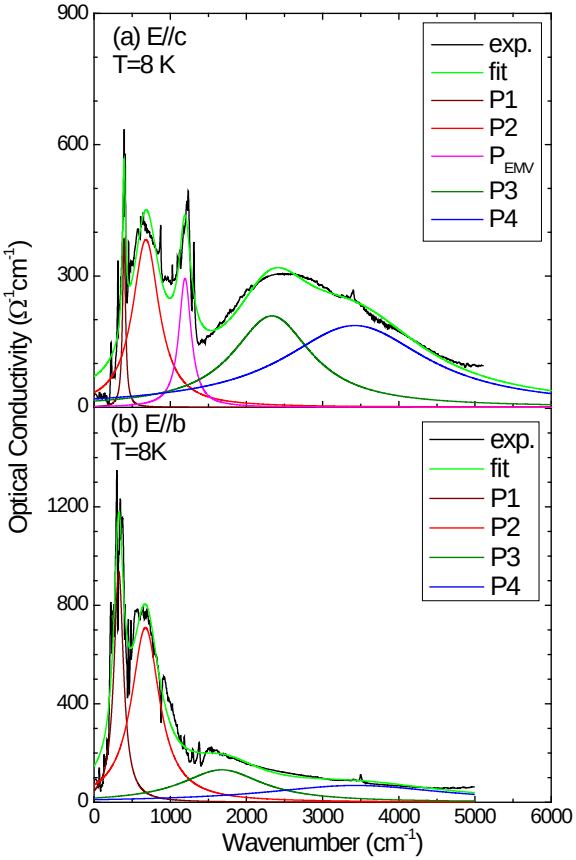

FIG. 11. Lorentz function fits of electronic bands in the spectra of δ-(BEDT-TTF)$_4$(ABS)·4H$_2$O at T=8 K for

polarization (a) parallel and (b) perpendicular to the BEDT-TTF stacks.

Nevertheless, since the stacks possess a zigzag structure (Fig. 12), it is not easy to indicate molecules between which this transition occurs. However, considering HOMO⋯HOMO interaction energies [10], it is possible that P_4 for *E//b* corresponds to transition between A molecules located in neighboring stacks. This A-A interaction grows from 0.1684 eV at 293 K to 0.2388 eV at 15 K, being thus responsible for the abrupt increase of the ν_3 intensity <85 K [Fig. 6(c)]. At ambient temperature, the P_3 band is observed at nearly the same frequency (2050 and 2070 cm^{-1}) for both perpendicular polarizations. We relate the P_3 feature to the transition between Hubbard bands. The x-ray data at 15 K indicate that the molecule B is charge rich, and A is charge poor [10]; therefore, the transition energy between B and A equals the Hubbard energies V_c and V_b along directions *c* and *b*, respectively (Fig. 12). The V_c and V_b energies are nearly the same at ambient temperature but show considerable difference <85 K due to the abrupt

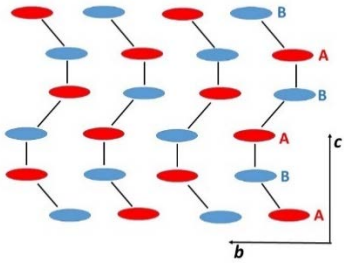

FIG. 12. Zigzag stacks of BEDT-TTF in δ-(BEDT-TTF)$_4$(ABS)·4H$_2$O. The charge-rich B (blue) and charge-poor A (red) molecules are arranged in stripes along the *c* axis below T_{MI}=85 K.

increase of interstack interactions. The band P_2 (690 cm^{-1} for *E//c* and 1140 cm^{-1} for *E//b* at 293 K) can be related to transitions between the electronic states at the Fermi level and the Hubbard bands. In other BEDT-TTF salts with ¼-band filling, this electronic absorption is observed in the region 700-500 cm^{-1} [29,37]. At room temperature, the P_1 band, assigned to short-range CO fluctuations, is located at a higher frequency for *E//b* (600 cm^{-1}) in comparison with *E//c* (330 cm^{-1}), while at 15 K, these frequencies are very close, providing thus additional evidence of a considerable increase of interstack interactions. In other ¼-filled BEDT-TTF salts, this band is in the range 100-300 cm^{-1} [26,32].

IV. CONCLUSIONS

In comparison with the other ¼-filled two-dimensional organic conductors showing a CO state, δ-(BEDT-TTF)$_4$(ABS)·4H$_2$O is a particular case for two reasons: (i) it is a δ-type salt with specific zigzag stacks of BEDT-TTF donors, (ii) the metal-insulator transition due to CO is evidently related with both the intersite Coulomb repulsion and the reorganization of hydrogen bond network existing inside insulating acceptor layers and between donors and acceptors [10]. Our IR studies provide clear evidence of these processes and additionally indicate the existence of strong charge fluctuations both in the metallic and insulating phases. It is important that, already at ambient temperature, charge is not uniformly distributed among A and B molecules ($2\delta\approx+0.05e$), most probably because of strong donor-acceptor interactions, and moreover, there exist significant short-range fluctuations between metallic and CO insulating state with $2\delta\approx+0.19e$. Upon cooling, these fluctuations grow (i.e., the short-living CO domains are larger and larger), and below the metal-insulator transition (T_{MI}=85 K), the CO state is formed with $2\delta\approx+0.25e$, but the fluctuations do not disappear, i.e., the domains with $2\delta\approx+0.08e$ still exist. Simultaneously, our IR data yield evidence of reorganization of the hydrogen bond network in insulating layers and modification of donor-acceptor interactions. It is also important that the IR data give evidence that the CO transition is associated with considerable increase of interactions between the zigzag stacks of BEDT-TTF, in agreement with the crystallographic studies and calculations of the HOMO⋯HOMO interaction energies [10]. Finally, it should be emphasized that the vibrational feature, associated with the interaction of the C=C stretching $\nu_3(a_g)$ phonon mode with electrons, is not only observed for polarization parallel to the stacks but also for the perpendicular direction. It implies that the $\nu_3(a_g)$ mode couples not only with intradimer charge transfer in the BEDT-TTF stacks but also with the interstack charge transfer. It is interesting that the intensity of the $\nu_3(a_g)$ band considerably grows when interaction between neighboring stacks increases because of the phase transition.

In δ-(BEDT-TTF)$_4$(ABS)·4H$_2$O, the strong charge fluctuations exist in a broad temperature range above and below the CO temperature, as it was observed in other BEDT-TTF salts, in particular in those where superconducting ground states were discovered [26,38,39]. Thus, it supports common opinion that physical properties of many strongly correlated ¼-filled BEDT-TTF conductors cannot be understood without considering the charge fluctuations.

ACKNOWLEDGMENT

The study was partially supported by the Deutscher Akademischer Austauschdienst (German Academic Exchange Service) ID: 5714349.

[1] N. Toyota, M. Lang, J. Müller, *Low-Dimensional Molecular Metals*, Series Volume 154 (Springer-Verlag Berlin, Heidelberg, 2007).

[2] R. T. Clay, S. Mazumdar, Phys. Rep. **788**, 1 (2018).

[3] M. Dressel and S. Tomić, Adv. Phys. **69**, 1 (2020).

[4] H. Seo, J. Phys. Soc. Jpn. **69**, 805 (2000).

[5] P. Alemany, J.-P. Pouget, and E. Canadell, Phys. Rev. B **85**, 195118 (2012).

[6] P. Alemany, J.-P. Pouget, and E. Canadell, J. Phys.: Condens. Matter **27**(46), 465702 (2015).

[7] J.-P. Pouget, P. Alemany, and E. Canadell, Mater. Horiz. **5**, 590 (2018).

[8] M. Dressel, and N. Drichko, Chem. Rev. **104**, 5689 (2004).

[9] K. Yakushi, Crystals **2**, 1291 (2012).

[10] F. Camerel, G. Le Helloco, T. Guizouarn, O. Jeannin, M. Fourmigué, A. Frąckowiak, I. Olejniczak, R. Świetlik, A. Marino, E. Collet, L. Toupet, P. Auban-Senzier, and E. Canadell, Cryst. Growth Des. **13**, 5135 (2013).

[11] T. Mori, Bull. Chem. Soc. Jpn. **72**, 2011 (1999).

[12] M. E. Kozlov, K. I. Pochodnia, and A. A. Yurchenko, Spectrochim. Acta A **43**, 323 (1987).

[13] M. E. Kozlov, K. I. Pochodnia, and A. A. Yurchenko, Spectrochim. Acta A **45**, 437 (1989).

[14] T. Yamamoto, M. Uruichi, K. Yamamoto, K. Yakushi, A. Kawamoto, and H. Taniguchi, J. Phys. Chem. B **109**, 15226 (2005).

[15] M. Dressel and G. Grüner, *Electrodynamics of Solids* (Cambridge University Press, Cambridge, 2002).

[16] See Supplemental Material at http://link.aps.org/supplemental/10.1103/PhysRevB.104.184104 for infrared and Raman spectra, tables with collected modes frequency, and further description.

[17] Y. Yue, K. Yamamoto, M. Uruichi, C. Nakano, K. Yakushi, S. Yamada, T. Hiejima, and A. Kawamoto, Phys. Rev. B **82**, 075134 (2010).

[18] S. Moroto, K.-I. Hiraki, Y. Takano, Y. Kubo, T. Takahashi, H.M. Yamamot, and T. Nakamura, J. Phys. IV France **114**, 339 (2004).

[19] A. Girlando, M. Masino, A. Brillante, R. G. Della Valle, and E. Venuti, *Horizons in Superconductivity Research*, (Nova Science Publishers, New York, 2003).

[20] A. Girlando, J. Phys. Chem. C **115**, 19371 (2011).

[21] J. L. Musfeldt, R. Świetlik, I. Olejniczak, J. E. Eldridge, and U. Geiser, Phys. Rev. B **72**, 014516 (2005).

[22] J. M. Williams, M.-H.Whangbo, A. J. Schultz, T. J. Emge, and M. A. Beno, J. Am. Chem. Soc. **109**, 90 (1987).

[23] T. Sugano, H. Hayashi, M. Kinoshita, K. Nishikida, Phys. Rev. B **39**, 11387 (1989).

[24] A. Girlando, M. Masino, S. Kaiser, Y. Sun, N. Drichko, M. Dressel, and H. Mori, Phys. Status Solidi B **249**, 953 (2012).

[25] A. Girlando, M. Masino, J. A. Schlueter, N. Drichko, S. Kaiser, and M. Dressel, Phys. Rev. B **89**, 174503 (2014).

[26] S. Kaiser, M. Dressel, Y. Sun, A. Greco, J. A. Schlueter, G. L. Gard, and N. Drichko, Phys. Rev. Lett. **105**, 206402 (2010).

[27] N. Tajima, M. Tamura, Y. Nishio, K. Kajita, and Y. Iye, J. Phys. Soc. Jpn. **69**, 543 (2000).

[28] K. Takenaka, M. Tamura, N. Tajima, H. Takagi, J. Nohara, and S. Sugai, Phys. Rev. Lett. **95**, 227801 (2005).

[29] N. Drichko, M. Dressel, C. A. Kuntscher, A. Pashkin, A. Greco, J. Merino, and J. Schlueter, Phys. Rev. B **74**, 235121 (2006).

[30] D. Faltermeier, J. Barz, M. Dumm, M. Dressel, N. Drichko, B. Petrov, V. Semkin, R. Vlasova, C. Meźière, and P. Batail, Phys. Rev. B **76**, 165113 (2007).

[31] M. Dumm, D. Faltermeier, N. Drichko, M. Dressel, C. Meźière, and P. Batail, Phys. Rev. B **79**, 195106 (2009).

[32] K. Hashimoto, S. C. Zhan, R. Kobayashi, S. Iguchi, N. Yoneyama, T. Moriwaki, Y. Ikemoto, and T. Sasaki, Phys. Rev. B **89**, 085107 (2014).

[33] A. Pustogov, K. Treptow, A. Rohweer, Y. Saito, M. Sanz Alonso, A. Löhle, J.A. Schluter, and M. Dressel, Phys. Rev. B **99**, 155144 (2019).

[34] C. Clauss, N. Drichko, D. Schweitzer, and M. Dressel, Physica B **405**, S144 (2010).

[35] W. Li, E. Rose, M.V. Tran, R. Hübner, A. Łapiński, R. Świetlik, S. A. Torunova, E.I. Zhilyaeva, R.N. Lyubovskaya, and M. Dressel, J. Chem. Phys. **147**, 064503 (2017).

[36] A. Pustogow, Y. Saito, A. Löhle, M. Sanz Alonso, A. Kawamoto, V. Dobrosavljević, M. Dressel, and S. Fratini, Nat. Commun. **12**, 1571 (2021).

[37] J. Merino, A. Greco, N. Drichko, and M. Dressel, Phys. Rev. Lett. **96**, 216402 (2006).

[38] W. Lubczynski, S. V. Demishev, J. Singleton, J. M. Caulfield, L. Du Croo de Jongh, C. J. Kepert, S. J. Blundell, W. Hayes, M. Kurmoo, and P. Day, J. Phys.: Condens. Matter **8**(33), 6005 (1996).

[39] J. Merino and R. H. McKenzie, Phys. Rev. Lett. **87**, 237002 (2001).